 doi:10.20944/preprints202010.0394.v1

Article

TOWARDS THE NEXT GENERATION OF TSUNAMI IMPACT SIMULATIONS

Simone Marras [1,‡], **Kyle T. Mandli** [2,‡]

[1] New Jersey Institute of Technology; smarras@njit.edu
[2] Columbia University; kyle.mandli@columbia.edu
* Correspondence: smarras@njit.edu
‡ These authors contributed equally to this work.

Received: date; Accepted: date; Published: date

Abstract: The approach to tsunami modeling and simulation has changed in the past few years more than it had in the previous two decades. This brief review describes why this modeling shift is happening and attempts to provide some insight into the future of computational tsunami research.

Keywords: Tsunami Modeling; Tsunami Simulations; Numerical Methods

1. Introduction

Figure 1. Pieces of the Tōhoku multi-billion dollar tsunami protection wall after a level-2 tsunami his the coasts of Japan in 2011. While each individual concrete section of the wall did not suffer significant damage, the erosion at the foundations of the wall happened so quickly that the concrete barrier simply fell (Picture from [1].)

The failure of a multi-billion dollar wall designed to protect the Tōhoku coasts of Japan (Figure 1) from a level-2 tsunami (i.e. infrequent but highly destructive) in 2011 has triggered an important debate about alternative approaches to tsunami risk reduction. This debate is on-going and has attracted broad media attention worldwide (Reuters [2], The Guardian [3], The Economist [4], The New York Times [5], Wired [6]). The question whether a wall is the best solution to tsunami mitigation lies in the significant expense required for a wall that does not necessarily guarantee protection from big tsunamis. A massive concrete wall also suggests a misleading sense of full protection that may prevent the affected communities from prompt evacuation [7], as sadly experienced in Tōhoku. Even when cost

Preprints (www.preprints.org) | NOT PEER-REVIEWED | Posted: 19 October 2020 doi:10.20944/preprints202010.0394.v1

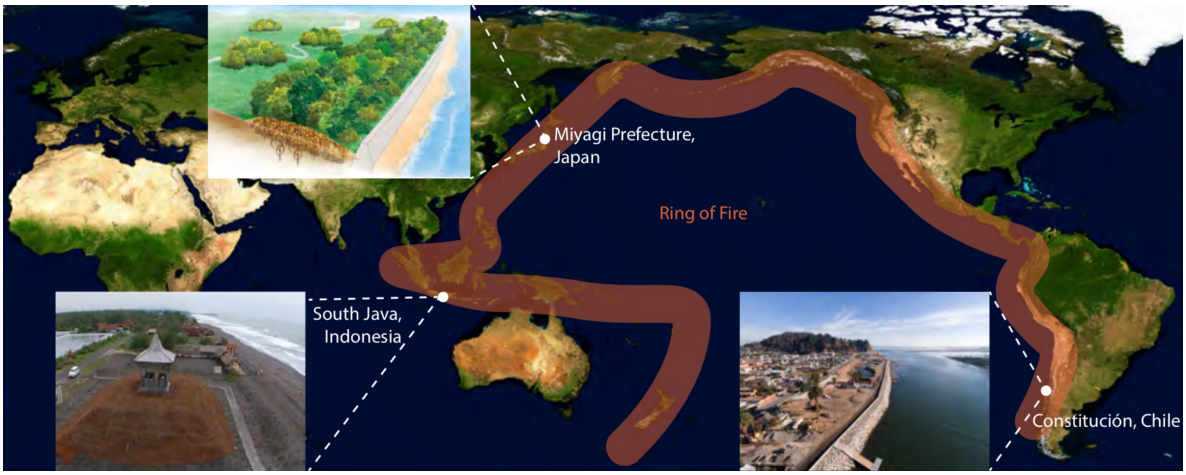

Figure 2. Map of the *Ring of Fire*, the longest coastal stretches that are most likely impacted by large tsunamis. Some tsunami mitigation parks are being constructed in South Java, Indonesia (Image: Indonesia Ministry of Marine Affairs and Fisheries), Miyagi Prefecture, Japan (Image: the Morino Project), and Constitución, Chile (Image: Architect Magazine). Adapted from [13].

is not the main constraint—consider Japan whose G.D.P. accounts for the 4.22% of the world economy, versus Indonesia's 0.93%, or Chile's 0.24%—relying on traditional concrete based solutions alone may not be desirable or sustainable, partly because of their potential long-term negative impact on the population [2], coastal ecosystems [8–10], and shoreline stability [11,12]. For these reasons, decision makers and engineers are increasingly considering protection solutions that rely on green designs as sustainable and effective alternatives to seawalls. These designs, which are spreading along the *Ring of Fire* as shown in Figure 2, are usually man-made hillscapes erected on the shoreline to protect the communities behind them by partially dissipating and partially reflecting the tsunami energy [13]. Unlike walls, these protective solutions do not give a false expectation of full protection because they are not meant to block the flow from reaching shore; instead, they are designed to let the flow through while dissipating its energy and, hence, allow the affected population to gain precious evacuation time. It is expected that similar solutions are likely to be proposed for protection from storm surge to diminish the risk of the devastation that hurricanes as strong as the recent Sandy and Katrina may cause.

While the numerical capabilities to model tsunamis in the deep ocean are well established and mature, as it will be further pointed out throughout this review it is still not the case for the modeling of tsunami-shore interaction once the wave propagates inland. The limit lies in the level of detail necessary to correctly estimate the forces involved. In this respect, in only five years since the review by Behrens and Dias [14], important steps towards high fidelity tsunami modeling at all scales have been made, contributing to further advance the forecast of tsunami impacts as envisioned by Bernard et al. [15] ten years earlier. This review describes the different approaches to tsunami modeling and simulation used to date. It will underline their properties and limits of validity to justify the ever increasing use of the 3D Navier-Stokes equations as the ultimate tool to study the tsunami boundary layer and run up.

The multi-scale nature of tsunami dynamics makes their study in a laboratory setting challenging [16,17]. For this reason, and supported by ever cheaper computing power and data storage, numerical modeling and simulation has become the most widely utilized tool for large-scale tsunami modeling and analysis [18]. Numerical modeling has shown to be effective to simulate tsunami generation (e.g., [19–23]), propagation (e.g., [24–26]), and coastal inundation [13,27–30], although the problem of inundation is still partially open when it comes to its numerical treatment (see, e.g., [31–35] and references therein).

Preprints (www.preprints.org) | NOT PEER-REVIEWED | Posted: 19 October 2020 doi:10.20944/preprints202010.0394.v1

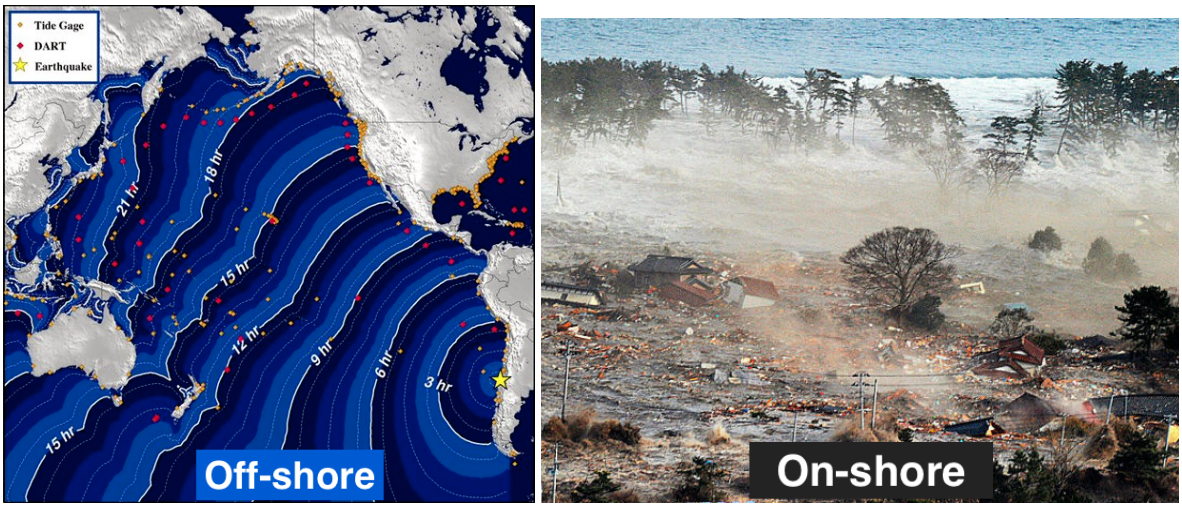

Figure 3. The off-shore tsunami is, effectively, a two-dimensional long-wave (top, Chilean tsunami, 2010). On-shore, however, it becomes turbulent and multi-phase –water, sand, dirt, debris– (right, Tōhoku tsunami, Japan, 2011). Left: adapted from NOAA Tsunami Warning System. Right: unknown source.

The effects of isolated components such as bathymetry and vegetation have been studied for idealized one-dimensional (1D) and two-dimensional (2D) settings using numerical simulations for years. For example, in [13,27,36–38], 1D and 2D shallow water models were used to demonstrate that the non-linearity of tsunami waves has a significant effect on the on-shore flow velocities and propagation. Many inundation modeling efforts aim to obtain an accurate prediction of the water elevation level. While these models typically do a good job at obtaining representative values of inundation levels, their correct prediction of water level seldom translates into the accurate prediction of the forces at play [39,40].

The evaluation of a tsunami from the point of view of wave breaking, turbulence, erosion, and sediment entrainment is computationally demanding. Why is this the case? A tsunami is a naturally multi-scale phenomenon whose characteristic length scales range from the planetary scale spanning oceans to the small scales of turbulence. In the open ocean it is, effectively, a fast moving two-dimensional long wave that can travel undisturbed for thousands of kilometers and can be accurately described by the 2D non-linear shallow water equations. On the other hand, as the flow approaches the shore and moves inland, its three-dimensionality and turbulent nature become important, with boundary layer dynamics that contribute to an important shear-driven erosion and sediment transport (See Figure 3). As the tsunami advances further inland, sand, dirt, vegetation, and other debris are scoured off of the sea bed, transported, and deposited along its path, potentially leading to important coastal morphological changes (e.g., [41–46]). By construction, however, the shallow water equations are not apt to model such complex flows, although they have been used in the context of erosion by [44,47–49]. Towards an understanding of the possible limitations of the shallow water equations for a fine-grained tsunami modeling, Qin et al. [50] compared the 3D Reynolds-Averaged Navier-Stokes (RANS) solution of a turbulent propagating bore using OpenFOAM [51] against the 2D shallow water solution of the same problem using GeoClaw[52]; Qin et al. demonstrated that a 3D model for turbulent flows is necessary to correctly predict tsunami inundation and the fluid forces involved. Among the first numerical studies that attempted to model tsunami run-up as the solution of the Navier-Stokes equations we find the 2D simulations by Hsiao and Lin [53] in 2011 and by Larsen and Fuhrman [54,55] who, in 2019, underlined the growing need for high-fidelity and multi-scale models to study tsunami risk and inland propagation. Furthermore, the RANS equations classically used for engineering turbulence modeling were shown to over-produce turbulence beneath surface waves [56], hence suggesting the need for high-fidelity turbulence models such as large eddy

Preprints (www.preprints.org) | NOT PEER-REVIEWED | Posted: 19 October 2020 doi:10.20944/preprints202010.0394.v1

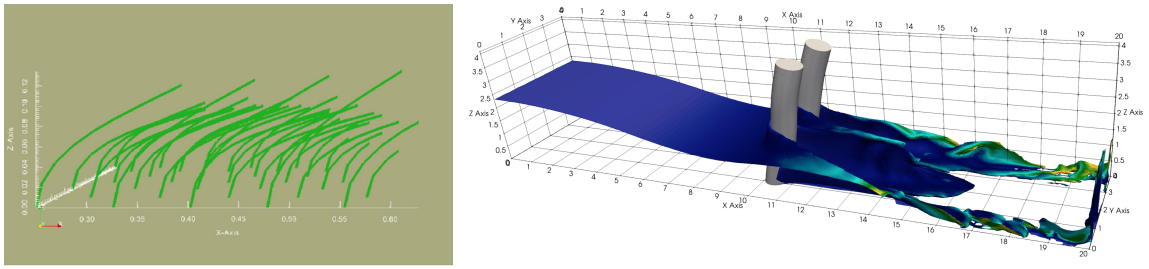

Figure 4. Two examples of flexible vegetation in a three-dimensional flow at large Reynolds number. Left: bent idealized 1D vegetation submerged in a channel flow (Adapted from [84]). Right: two-way fluid-structure interaction model of 3D idealized trees in a dam break triggered flow (Image courtesy of Abhishek Mukherjee.)

simulation. Large eddy simulation was used in the context of plunging breakers by Christensen [57] who underlined the numerical challenges of models in reproducing experimental results on the surf zone dynamics. Much attention has been given to run up; however, not enough work has addressed the analysis of the interaction of the tsunami with the built environment and vegetation, and of the erosion caused by large tsunamis [55] which is critical to improving the prediction of inundation. Modeling erosion with shallow water models is difficult due to the lack of velocity shear in these models; but shear is the driving mechanism of erosion and entrainment. Moreover, the modeling of the dynamics of the near-bed region and of erosion is still an open challenge in coastal engineering because it is governed by important particle-particle and particle–fluid interactions [58]; if analyzed by means of fine-grained numerical models, grain-resolving simulations are necessary [59,60].

Proper fine-grained modeling is important beyond erosion. In the context of tsunami impact mitigation analysis, the next frontier may lie in the detailed simulation of vegetation–tsunami and vegetation–morphology interactions. In light of the pioneering findings by the U.S. Army Corps of Engineers that vegetation may act as a bio-shield against flooding from storm surges [61,62], the designs of tsunami mitigation solutions around the world often incorporate vegetation. Significant experimental and numerical work has been done to analyse the effect of vegetation on wind waves, currents and, albeit less so, tsunamis (e.g., [63–72]), particularly in the context of steady flows [73]. After the 2004 tsunami in Sumatra, Bayas et al. [74] estimated that vegetation along the west coast of Aceh may have reduced casualties by 5%. The benefits of coastal vegetation are not limited to attenuation. It is well known that bathymetry, topography, and coastal geomorphology (rivers, canals, and barrier islands) have a profound effect on run-up for both tsunamis [13] and storm surge [75–78]. Furthermore, the presence of vegetation alters sediment-transport processes and landform evolution [79–83]. The modeling of the interaction between the tsunami and vegetation is numerically difficult because of the flexible nature of vegetation. Efforts have been made to include the effect of flexible vegetation on the flow. Examples of one- and two-way coupling of the flow with the the dynamics of vegetation can be found in the recent work by Mattis et al. [84,85] and Mukherjee et al. [86] who, for the first time, used fluid-structure interaction algorithms to study the effect of deformation of idealized trees on the flow (See Figure 4).

2. Mathematical representations

While the most complete model to describe a tsunami as a highly turbulent free surface flow is given by the Navier-Stokes equations of incompressible flows, simpler models of wave propagation have been successfully adopted for decades to study tsunami propagation in the open ocean and run-up [14,18]. In this section, we introduce the different models, underline their properties and limits of validity and justify the ever increasing use of the full 3D Navier-Stokes equations to study the boundary layer and run up.

Preprints (www.preprints.org) | NOT PEER-REVIEWED | Posted: 19 October 2020 doi:10.20944/preprints202010.0394.v1

2.1. Depth-Averaged Models

The first set of approximations that we will consider are the large class of equations characterized by averaging through the depth of the water column in the gravity centered coordinate system (See Fig. 5). This precludes modifications that would handle steeper terrain in favor of reducing complexity but should be noted as an alternative for simple topographical features. We will also forgo analysis of layered depth-averaged models as though they have unique properties and largely follow the same derivation.

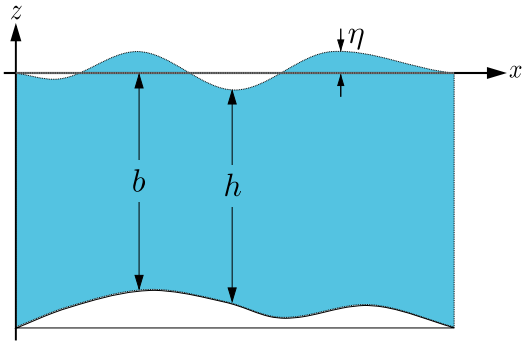

Figure 5. Gravity centered, depth averaged coordinate system for the shallow water equations. Here h is the depth of the water column, η the difference between a defined datum, commonly a given sea-level, and the sea-surface, and b the bathymetry surface as measured from the same datum.

2.1.1. Scaled Equations

We first start with the inviscid version of the 2D Navier-Stokes equations (i.e. the Euler equations) of incompressible flows, one vertical and horizontal dimension, where we will ignore one of the horizontal directions for simplicity of notation and without loss of generality. With this setup and assuming a free surface and non-flat bottom boundary we have the equations

$$\begin{aligned} u_x + w_z &= 0 \\ u_t + (u^2)_x + (uw)_z &= -\frac{1}{\rho} P_x \\ w_t + (uw)_x + (w^2)_z &= -\frac{1}{\rho} P_z - g \end{aligned} \tag{1}$$

with the boundary conditions

$$\begin{cases} w = \eta_t + u\eta_x \\ P = P_a \end{cases} \qquad z = \eta \tag{2}$$

$$w = ub_x \qquad z = b \tag{3}$$

where the velocity is represented by u in the horizontal direction, w in the vertical, ρ the density of water, P the pressure, which includes non-hydrostatic components at this juncture, and g the gravitational acceleration.

The first step in defining and justifying the depth-averaged equations lies in the non-dimensionalization assumptions made during their definition. Because of this we will be explicit about these assumptions as they will play an important role later on. The primary scalings are

$$\frac{x}{\lambda} = \tilde{x} \qquad \frac{z}{a} = \tilde{z} \qquad \frac{t}{T} = \tilde{t} \tag{4}$$

where λ is a length scale, often taken as the characteristic wave-length of the waves involved, a the characteristic depth that the wave is propagating through, T the characteristic time-scale or period of

Preprints (www.preprints.org) | NOT PEER-REVIEWED | Posted: 19 October 2020 doi:10.20944/preprints202010.0394.v1

the wave, and P_0 the pressure normalization, usually taken to be atmospheric pressure. With these values defined we can also normalize the velocities and P such that

$$\frac{u}{U} = \tilde{u} \qquad \frac{w}{W} = \tilde{w} \qquad \frac{P}{P_0} = \tilde{P} \tag{5}$$

where the non-dimensional quantities are those with $\tilde{\cdot}$. Introducing then the traditional shallow water parameter

$$\epsilon = \frac{a}{\lambda}$$

we can write the velocity and temporal normalizations as

$$U = \sqrt{ga} \qquad W = \epsilon U \qquad T = \frac{\lambda}{U}.$$

Applying these scaling to (1) and simplifying we are lead to the system of equations

$$\tilde{u}_{\tilde{x}} + \tilde{w}_{\tilde{z}} = 0 \tag{6}$$
$$\tilde{u}_{\tilde{t}} + (\tilde{u}^2)_{\tilde{x}} + (\tilde{u}\tilde{w})_{\tilde{z}} = -\tilde{P}_{\tilde{x}} \tag{7}$$
$$\epsilon^2 \left(\tilde{w}_{\tilde{t}} + (\tilde{u}\tilde{w})_{\tilde{x}} + (\tilde{w}^2)_{\tilde{z}} \right) = -\tilde{P}_{\tilde{z}} - g \tag{8}$$

where we have also assumed that $\frac{P_0}{\rho U^2} = 1$ without loss of generality. For the boundary conditions we introduce a new scaling, $\frac{\eta}{\delta} = \tilde{\eta}$ and $\frac{b}{\beta} = \tilde{b}$, which for the top boundary results in

$$\epsilon \frac{\lambda}{\delta} \tilde{w} = \tilde{\eta}_{\tilde{t}} + \tilde{u}\tilde{\eta}_{\tilde{x}} \tag{9}$$
$$\epsilon \frac{\lambda}{\beta} \tilde{w} = \tilde{u}\tilde{b}_{\tilde{x}}. \tag{10}$$

For the upper boundary condition, if $\frac{\delta}{\lambda} = \mathcal{O}(\epsilon)$, the boundary condition is all of the same order. This is probably not the case as $\delta \ll a$ unless in very shallow water but also should be noted for later.

The lower boundary condition is a similar situation, if $\frac{\beta}{\lambda} = \mathcal{O}(\epsilon)$ the boundary condition is all of the same order. In the case of the bathymetry scale, this is probably the case as the bathymetry will vary on the scale of the depth scale a. The final non-dimensionalized equations are then (dropping the $\tilde{\cdot}$):

$$\begin{aligned} u_x + w_z &= 0 \\ u_t + (u^2)_x + (uw)_z &= -P_x \\ \epsilon^2 \left(w_t + (uw)_x + (w^2)_z \right) &= -P_z - 1 \end{aligned} \tag{11}$$

with the boundary conditions

$$\begin{aligned} \epsilon \frac{\lambda}{\delta} w = \eta_t + u\eta_x \qquad P = P'_a \qquad z = \eta \\ \epsilon \frac{\lambda}{\beta} w = u b_x \qquad\qquad\qquad z = b \end{aligned} \tag{12}$$

where P'_a is the appropriately scaled atmospheric pressure condition.

2.1.2. Depth Integration

The next step to deriving the shallow water and similar equations is to depth integrate (11). Here we will skip many of the details other than to point out two important assumptions that are often misrepresented.

Preprints (www.preprints.org) | NOT PEER-REVIEWED | Posted: 19 October 2020 doi:10.20944/preprints202010.0394.v1

Continuing on the first step is to integrate the incompressibility equation in (11) such that we find

$$\int_b^\eta (u_x + w_z)\, dz = 0 \quad \Rightarrow \quad h_t + \frac{\partial}{\partial x}\int_b^\eta u dz = 0. \tag{13}$$

The next equation to be integrated is the horizontal momentum equation. For this we will first introduce the assumption that the total pressure P can be split up additively into an hydrostatic and non-hydrostatic component such that

$$P(x,z,t) = P_a + (\eta - z) + p$$

where now $p(x,z,t)$ is that non-hydrostatic component. Integrating the left-hand-side of this equation then we find

$$\int_b^\eta \left(u_t + (u^2)_x + (uw)_z\right) dz \quad \Rightarrow \quad \frac{\partial}{\partial t}\int_b^\eta u dz + \frac{\partial}{\partial x}\left(\int_b^\eta u^2 dz + \int_b^\eta p dz + \frac{1}{2}h^2\right)$$

where we have simplified the notation using our average values making sure to maintain the non-commutativity of the average and squaring operators. For the right-hand-side of the the horizontal momentum equation we similarly conclude that

$$-\int_b^\eta (P_a + (\eta - z) + p)_x dz \quad \Rightarrow \quad -b_x(h + p|_{z=b}).$$

Finally we also integrate the vertical momentum equation through the depth. This is very similar to the horizontal equations leading to

$$\epsilon^2 \int_b^\eta \left(w_t + (uw)_x + (w^2)_z\right) dz \quad \Rightarrow \quad \epsilon^2\left(\frac{\partial}{\partial t}\int_b^\eta w dz + \frac{\partial}{\partial x}\int_b^\eta uw dz\right)$$

for the left-hand-side and

$$-\int_b^\eta (P_a + (\eta - z) + p)_z + 1)\, dz \quad \Rightarrow \quad p|_{z=b}$$

for the right-hand side of the equation.

Putting all this together leads us to the vertically integrated equations

$$\begin{aligned} &h_t + \frac{\partial}{\partial x}\int_b^\eta u dz = 0 \\ &\frac{\partial}{\partial t}\int_b^\eta u dz + \frac{\partial}{\partial x}\left(\int_b^\eta u^2 dz + \int_b^\eta p dz + \frac{1}{2}h^2\right) = -b_x(h + p|_{z=b}) \\ &\epsilon^2\left(\frac{\partial}{\partial t}\int_b^\eta w dz + \frac{\partial}{\partial x}\int_b^\eta uw dz\right) = p|_{z=b}. \end{aligned} \tag{14}$$

At this juncture it is useful to start to introduce notation that indicates average quantities through the depths. We will denote these by

$$\begin{aligned} \overline{u} &= \frac{1}{h}\int_b^\eta u dz, & \overline{w} &= \frac{1}{h}\int_b^\eta w dz, \\ \overline{u^2} &= \frac{1}{h}\int_b^\eta u^2 dz, & \overline{w^2} &= \frac{1}{h}\int_b^\eta w^2 dz, \\ \overline{p} &= \frac{1}{h}\int_b^\eta p dx, \quad \text{and} & \overline{uw} &= \frac{1}{h}\int_b^\eta uw dz. \end{aligned} \tag{15}$$

Here in lies one of the critical misrepresentations of depth averaged models, that they assume constant velocity, or even more general quantities, throughout their vertical profiles. For example, in general

Preprints (www.preprints.org) | NOT PEER-REVIEWED | Posted: 19 October 2020 doi:10.20944/preprints202010.0394.v1

$\overline{u^2} \neq \overline{u}^2$. In fact we will make some assumptions about the commutativity of the averaging operator with others but this does not preclude the consideration of non-constant functions of the velocity for instance. This leads to the following system of equations,

$$\begin{aligned} &\frac{\partial}{\partial t}h + \frac{\partial}{\partial x}(h\overline{u}) = 0 \\ &\frac{\partial}{\partial t}(h\overline{u}) + \frac{\partial}{\partial x}\left(h\overline{u^2} + h\overline{p} + \frac{1}{2}h^2\right) = -(h + p|_{z=b})\frac{\partial b}{\partial x} \\ &\epsilon^2\left(\frac{\partial}{\partial t}(h\overline{w}) + \frac{\partial}{\partial x}(\overline{uw})\right) = p|_{z=b} \end{aligned} \tag{16}$$

One last equation for the pressure will be useful as it will give us a means to calculate $\overline{p}$ depending on the approximations that we will make in the next section. We can come to this equation by reconsidering the scaled vertical momentum equation and integrating from η to a vertical level $b + \alpha h$ where $\alpha \in [0, 1]$ leading to

$$\epsilon^2\left\{\frac{\partial}{\partial t}\int_{b+\alpha h}^{\eta} w dz + \frac{\partial}{\partial x}\int_{b+\alpha h}^{\eta} uw dz + \{w[\alpha(\eta_t + u\eta_x) + (1+\alpha)ub_x - w]\}|_{z=b+\alpha h}\right\} = p|_{z=b+\alpha h}.$$

2.1.3. Approximations

At this point we can use the equations from the previous section to derive a number of approximations commonly used in tsunami numerical modeling. This will not be exhaustive but rather suggestive to where this basic framework can be taken to derive and analyze the validity of these approximations.

The first of these approximations will assume that the averaging operator will commute with multiplication, e.g. $\overline{u}^2 \approx \overline{u^2}$. The terms that this ignores are often termed as *differential advection*; but note that this approximation does not imply that the velocity profiles are constant but rather that the averages commute. This can be important when comparing boundary layer physics for instance. Moving forward, this allows use to rewrite (17) and simplify notation so that

$$\begin{aligned} &h_t + (hu)_x = 0 \\ &(hu)_t + \left(hu^2 + hp + \frac{1}{2}h^2\right)_x = -(h + p|_{z=b})b_x \\ &\epsilon^2\left((hw)_t + (uw)_x\right) = p|_{z=b} \end{aligned} \tag{17}$$

where we have also now dropped the $\overline{\cdot}$ notation.

Shallow Water

Finally for the shallow water equations we simply need to assume that the shallow water parameter $\epsilon \ll 1$ implying that $0 = p|_{z=b}$. Since the non-hydrostatic pressure is defined such that $p(x, \eta, t) = 0$ we can show that $\overline{p} = 0$ therefore implying that (17) become

$$\begin{aligned} &h_t + (hu)_x = 0 \\ &(hu)_t + \left(hu^2 + \frac{1}{2}h^2\right)_x = -hb_x, \end{aligned} \tag{18}$$

which are of course the traditional, non-dimensionalized shallow water equations. Note that (2.1.2) can be used here to show that $\overline{p} = 0$ is in fact true here.

Preprints (www.preprints.org) | NOT PEER-REVIEWED | Posted: 19 October 2020 doi:10.20944/preprints202010.0394.v1

Not So Shallow Equations

The next perhaps logical step is to maintain the assumption that differential advection is still small and therefore averages commute but that vertical momentum is not as ignorable as before, i.e. $\epsilon \geq \mathcal{O}(1)$. Instead we might make some assumptions about the depth profile of w and use that to derive a form of a closure expression for the non-hydrostatic pressure. Here we will give one example of an analysis where we assume that w has a linear profile through the depth along with the equations that arise due to this assumption.

First if w is linear in z we can use the incompressibility condition to find

$$w(x,z,t) = w(x,t) - u_x z.$$

The crux of these calculations are then to compute the expressions for $\overline{w}$ and $\overline{p}$. Leaving out the tedious details of these calculations but reporting the results the final equations with these assumptions leads to

$$\begin{aligned} &h_t + (hu)_x = 0, \\ &(hu)_t + \left(hu^2 + \frac{1}{2}h^2 + h\overline{p}\right)_x = -b_x(h + p|_{z=b}), \text{ and} \\ &(hw)_t + (huw)_x - \left[\left(hu_x\left(\frac{1}{2}h + b\right)\right)_t + \left(huu_x\left(\frac{1}{2}h + b\right)\right)_x\right] = p|_{z=b}, \end{aligned} \tag{19}$$

where

$$\begin{aligned} \overline{p} = \frac{\epsilon^2}{h}\Bigg\{&\frac{\partial}{\partial t}\left(\frac{1}{2}hw + \frac{1}{2}u_x hb + \frac{1}{3}u_x h^2\right) + \frac{\partial}{\partial x}\left(\frac{1}{2}huw + \frac{1}{4}(u^2)_x hb + \frac{1}{6}(u^2)_x h^2\right) \\ &- \frac{3}{2}w^2 + \frac{3}{2}uwb_x + 3bwu_x - \frac{3}{2}b^2(u_x)^2 - \frac{3}{4}((ub)^2)_x + \frac{11}{6}hwu_x \\ &-\frac{3}{2}hb(u_x)^2 - \frac{1}{4}h(bu^2)_x - \frac{2}{3}(hu_x)^2 - \frac{1}{3}hb_x(u_x)^2\Bigg\} \end{aligned} \tag{20}$$

2.2. Navier-Stokes equations

All of the models above do a very good job at solving wave propagation and, when enhanced with an appropriate wetting-and-drying scheme, at simulating inundation. Nonetheless, they lack the three-dimensionality that allows for turbulence to be accounted for. During inundation, the interaction of the flow with the coastal features, erodible terrain, sediments, vegetation, and structures is such that the flow is fully turbulent, hence three-dimensional and characterized by shear. The correct estimation of the hydrodynamic forces responsible for the damages during run up requires a model that can capture these flow characteristics. The Navier-Stokes equations are the most complete model available to us if these flow features are to be considered. The 3D continuity and Navier-Stokes equations of incompressible viscous flows can be easily obtained by making the Euler equations 1, time dependent, by extending them to three spatial dimensions, and by including molecular viscosity. We write them as follows:

$$\begin{aligned} &u_x + v_y + w_z = 0 \\ &u_t + (u^2)_x + (uv)_y + (uw)_z = -\frac{1}{\rho}P_x + \nu(u_{xx} + u_{yy} + u_{zz}) \\ &v_t + (vu)_x + (v^2)_y + (vw)_z = -\frac{1}{\rho}P_y + \nu(v_{xx} + v_{yy} + v_{zz}) \\ &w_t + (wu)_x + (wv)_y + (w^2)_z = -\frac{1}{\rho}P_z + \nu(w_{xx} + w_{yy} + w_{zz}) - g \end{aligned} \tag{21}$$

While Equations (21) do model turbulent incompressible flows, its solution on a computational grid requires some attention with respect to the treatment of the viscous stresses. If we could afford to have an infinitely fine computational grid, we could solve them directly; an approach, this one,

Preprints (www.preprints.org) | NOT PEER-REVIEWED | Posted: 19 October 2020 doi:10.20944/preprints202010.0394.v1

Table 1. Some available tsunami models. Acronyms used in this table: *SW* Shallow Water, *B* Boussinesq, $N-S$ Navier-Stokes, *SPH* Smoothed Particle Hydrodynamics, *LES* Large Eddy Simulation, *WM* Wall Modeled LES, *RANS* Reynolds Averaged Navier-Stokes equations, *FSI* Fluid-Structure Interaction, *MP* Multi-Phase capabilities for erosion and sediment transport. The use of $2D(1/2)$ indicates that the model can run in two-layer modality [95]. Storm surge and ocean dynamics models are omitted.

Model	Space Dimensions	Equations	Turbulence	Wave breaking	*FSI*	*MP*
GeoCLAW [52]	$1D/2D/2D\frac{1}{2}$	*SW*	No	No	No	No
NUMA2D [96–98]	1D/2D	*SW*	No	No	No	No
MOST [99]	1D/2D	*SW*	No	No	No	No
TUNAMI [100]	1D/2D	*SW*	No	No	No	No
NAMI-DANCE[101]	1D/2D	*SW*	No	No	No	No
COMCOT [102]	1D/2D	*SW*	No	No	No	No
CEA [103,104]	1D/2D	*SW*	No	No	No	No
SELFE [105]	1D/2D	*SW*	No	No	No	No
TsunAWI [106]	1D/2D	*SW*	No	No	No	No
VOLNA [107]	1D/2D	*SW*	No	No	No	No
TsunaFlash [108]	1D/2D	*SW*	No	No	No	No
Delft3D [109]	1D/2D	*SW*	No	No	No	Yes
Basilisk [110]	2D/3D	*SW*	No	Yes	No	Yes
FUNWAVE [111,112]	1D/2D	*B*	No	No	No	No
COULWAVE [113,114]	2D	*B*	No	No	No	No
NEOWAVE [115]	2D	*B*	No	No	No	No
GPUSPH [116]	3D	*SPH*	No	Yes	No	No
SCHISM [90]	1D/2D/3D	$N-S$	*RANS*	Yes	No	No
COBRAS [87,88]	2D/3D	$N-S$	*RANS*	Yes	No	No
TSUNAMI3D [89]	2D/3D	$N-S$	*RANS*	Yes	No	No
waves2FOAM [54,55,91]	2D (tsunami)	$N-S$	*RANS*	Yes	No	No
Alya [86,117]	2D/3D	$N-S$	*LES/WM/RANS*	Yes	Yes	Yes

known as direct numerical simulation (DNS). However, even with the approaching era of exa-scale computing, DNS is much too costly to be viable for tsunami simulations[1]. Instead, by means of either a Reynolds averaging approach that gives rise to the RANS equations, or scale separation filtering in what is known as Large Eddy Simulation (LES), turbulence can be modeled with sufficient precision at a drastically reduced computational cost with respect to DNS. RANS was first used for tsunami run up simulation in the software COBRAS [87,88]. But it took approximately one more decade to become a popular choice to model tsunami generated turbulence. Examples of RANS tsunami models are described in [54,55,89–91]. In terms of solution cost, LES lies between DNS and RANS. Due to its computational cost, it is not popular among tsunami modelers yet although it was recently considered as an optimal choice to study breaking waves and run up in highly non-steady dynamics (e.g. [86]). As the era of exa-scale computing on hybrid CPU-GPU architectures is fast approaching, we expect LES to become the model of choice among tsunami inundation modelers. Some of the most common tsunami simulators are listed in Table 1.

The free surface in a model based on the solution of (21) is typically accounted for in either one of two ways: by means of a volume of fluid approach (in, e.g. [91,92]) or by a level-set tracking of the water-air interface in a two-fluid model (in, e.g., [86,93,94]). Both of these approaches make it natural to handle the wet-dry front as the flow reaches land; this is not the case for shallow-water equations whose numerical solution is challenged in wet-dry regions.

3. Numerical Solution

The equations described across this paper have been solved for decades using a wide range of numerical approximations. From the classical finite difference method (FD) used in, e.g. MOST [99], to

[1] The number of grid points in a computational grid necessary for DNS scales as the $(9/4)^{th}$ power of the Reynolds number.

Preprints (www.preprints.org) | NOT PEER-REVIEWED | Posted: 19 October 2020 doi:10.20944/preprints202010.0394.v1

finite volumes (FV; see, e.g. [25,52,95,107,118]), to the finite element method (FEM; e.g. [86,119]) and high-order continuous and discontinuous Galerkin methods (CG/DG; e.g. [13,26,33,94,106]), to the less common smoothed particle hydrodynamics method (SPH; e.g. used in GPUSPH [116]) that has been gaining popularity to model free surface flows in engineering and hydraulics from its origins in astrophysics.

Each numerical method comes with its advantages and disadvantages. FD are less costly than CG/DG, but they lack the geometrical flexibility of Galerkin methods and FV. CG/DG and FV are optimal for grid refinement [26,52,120] and are geometrically flexible to handle complex coastal lines; furthermore, CG/DG are inherently optimal for massive parallelism [121,122]. SPH is good at tracking the free surface of the three dimensional flow, but it is expensive and it is still unclear how to treat boundary layers. Regardless of the numerical method of approximation, the handling of the wet-dry interface to model inundation is still a difficult problem to solve, especially so for high-order methods as demonstrated by the extensive work on wetting and drying presented in, e.g., [31–35,123].

In summary, all these methods have their use case and there is no one that can rule them all. Similarly the adage "using the right tool for the job" holds here as much as it does when doing carpentry. It is important therefore to consider what metrics may lead to the decisions to chose one model over another. Among the most prominent are:

- Performance on the computing architecture being considered.
- Complexity of the physics needed. Here the difference between using a wall boundary condition at the shore and doing true wetting and drying may be significant as does the representation of true turbulent flow.
- Overall size of the problem considered. Are you interested in a single simulation or a large ensemble in order to take into account uncertainty.

These are of course only some of the issues but highlight the difficulties faced and the need for hybrid solver techniques to bridge the gaps between the advantages and disadvantages between solvers.

4. Towards a multi-scale framework from source to impact

It seems plausible, given the on-going research on all fronts from tsunami generation, propagation, to fine-scale run up, that the community of tsunami modelers will soon join forces to build a unified, all-scale framework to model a full tsunami event from source to impact (see, e.g. [21,124]). The all-scale idea is naïvely represented in Figure 6. The 3D Navier-Stokes solver is forced at the boundaries by the shallow water model of the tsunami moving off-shore, which is forced by an earthquake simulator or, in the case of landslide triggered tsunamis, landslide model. Arguably the most difficult and still unclear part of a modeling infrastructure of this type lies in the coupling across models. Coupling across models is an open field of research of its own (see, e.g. [125–128].) Parallel performance, data exchange, and time scale interactions, are among the difficulties to be overcome in designing coupling algorithms across software packages. We envision a major effort to optimize software coupling and make it efficient for costly tsunami simulations towards real-time modeling of a full tsunami event.

5. Conclusions

The current state of the field seems to indicate that the numerical tsunami modeling community is moving towards the high-fidelity modeling of tsunamis across scales. We expect an increasing effort to couple different models and allow the interaction of an earthquake simulator with the large scale dynamics in the open sea and fine scale dynamics in the coastal region, all within the same software infrastructure. While improved earthquake–tsunami modeling at the source, adaptive grid refinement, and ever faster and inexpensive hybrid high-performance computing (i.e. graphics processing units, GPUs) have contributed to the advancement of tsunami modeling at large scales, we are now witnessing the very beginning of a new tsunami modeling era; the introduction of high-fidelity simulations of inundation and enhanced coupling of software packages across all scales is finally

Preprints (www.preprints.org) | NOT PEER-REVIEWED | Posted: 19 October 2020 doi:10.20944/preprints202010.0394.v1

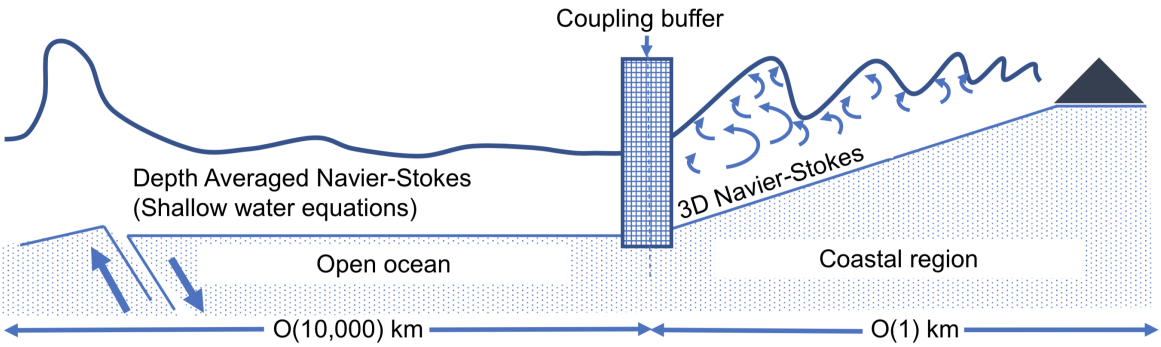

Figure 6. Representation of a comprehensive off-to–on-shore flow framework. The 3D Navier-Stokes solver is forced at the boundaries by the shallow water model of the tsunami off-shore, which is forced by an earthquake simulator.

leading the way towards real-time tsunami forecast as envisioned by Synolakis et al. [18] fifteen years ago.

While it is difficult to estimate how long it will be before a full scale tsunami simulation can be run in real time (or faster) on a laptop, the pace at which the necessary tools are being developed is fast. At risk of being too optimistic, current research leads us to think that such a tool may be available within the next fifteen years.

Author Contributions: S.M and K.M.contributed equally to the planning and writing of this review.

Conflicts of Interest: The authors declare no conflict of interest.

References

1. Renew Yamada. http://renewyamada.org, 2011.
2. Reuters. Seven years after tsunami, Japanese live uneasily with seawalls, 2018.
3. Guardian, T. After the tsunami: Japan's sea walls – in pictures, 2018.
4. Economist, T. The Great Wall of Japan, 2014.
5. Times, N.Y. Seawalls Offered Little Protection Against Tsunami?s Crushing Waves, 2011.
6. Wired, W. Ominous views of Japan's new concrete seawalls, 2018.
7. Nateghi, R.; Bricker, J.D.; Guikema, S.D.; Bessho, A. Statistical Analysis of the Effectiveness of Seawalls and Coastal Forests in Mitigating Tsunami Impacts in Iwate and Miyagi Prefectures. *PLoS ONE* **2016**, *11*.
8. Peterson, M.; Lowe, M. Implications of Cumulative Impacts to Estuarine and Marine Habitat Quality for Fish and Invertebrate Resources. *Rev. Fish. Sci.* **2009**, *17*, 505–523.
9. Dugan, J.; Hubbard, D. Ecological Effects of Coastal Armoring: A Summary of Recent Results for Exposed Sandy Beaches in Southern California. Puget Sound Shorelines and the Impacts of Armoring, U.S. Geol. Surv. Sci. Invest. Rep.; Shipman, H.; Dethier, M.; Gelfenbaum, G.; Fresh, K.; Dinicola, R., Eds., 2010.
10. Bulleri, F.; Chapman, M. The introduction of coastal infrastructure as a driver of change in marine environments. *J. Appl. Ecol.* **2010**, *47*.
11. Dean, R.G.; Dalrymple, R.A. *Coastal processes with engineering applications*; Cambridge University Press, 2002.
12. Komar, P. *Beach processes and sedimentation*; Prantice Hall, 1998.
13. Lunghino, B.; Santiago Tate, A.; Mazereeuw, M.; Muhari, A., G.F.; Marras, S.; Suckale, J. The protective benefits of tsunami mitigation parks and ramifications for their strategic design. *Proc. Nat. Acad. Sci. (PNAS)* **2020**, *1911857117*.
14. Behrens, J.; Dias, F. New computational methods in tsunami science. *Phil. Trans. R. Soc. A* **2015**, *373*, 20140382.
15.
16. Chen, J.; Huang, Z.; Jiang, C.; Deng, B.; Long, Y. An experimental study of changes of beach profile and mean grain size caused by tsunami-like waves. *J. Coast. Res.* **2012**, *28*, 1303–1312.

17. Jiang, C.; Chen, J.; Yao, Y.; Liu, J.; Deng, Y. Study on threshold motion of sediment and bedload transport by tsunami waves. *Ocean Eng.* **2015**, *100*, 97–106.
18. Synolakis, C.; Bernard, E. Tsunami science before and beyond boxing day. *Phil. Trans. Roy. Soc. Lond.* **2006**, *364*, 2231–2265.
19. Borrero, J.C.; Legg, M.R.; Synolakis, C.E. Tsunami sources in the southern California bight. *Geophysical Research Letters* **2004**, *31*.
20. Pelties, C.; de la Punte, P.; Ampuero, J.P.; Brietzke, G.; Käser, M. Three-dimensional dynamic rupture simulation with a high-order discontinuous Galerkin method on unstructured tetrahedral meshes. *J. Geophys. Res.* **2012**, *117*, 2156–2202.
21. López-Venegas, A.; Horrillo, J.; Pampell-Manis, A.; Huérfano, V.; Mercado, A. Advanced Tsunami Numerical Simulations and Energy Considerations by use of 3D-2D coupled Models: The October 11, 1918, Mona Passage Tsunami. *Pure App. Geophys.* **2014**, *171*, 2863–3174.
22. Galvez, P.; Ampuero, J.P.; Dalguer, L.; S.N., S.; Nissen-Meyer, T. Dynamic earthquake rupture modelled with an unstructured 3-D spectral element method applied to the 2011 M9 Tohoku earthquake. *Geophys. J. Int.* **2014**, *198*, 1222–1240.
23. Ulrich, T.; Vater, S.; Madden, E.; Behrens, J.; van Dinther, Y.; van Zelst, I.; Fielding, J.; Liang, C.; Gabriel, A.A. Coupled, Physics-Based Modeling Reveals Earthquake Displacements are Critical to the 2018 Palu, Sulawesi Tsunami. *Pure Appl. Geophys.* **2019**, *176*, 4069–4109.
24. Titov, V.; González, F.; Bernard, E.; Eble, M.C.; Mofjeld, H.; Newman, J.C.; Venturato, A. Real-Time Tsunami Forecasting: Challenges and Solutions. *Nat. Hazards* **2005**, *35*, 41–58.
25. LeVeque, R.; George, D.; Berger, M. Tsunami modelling with adaptively refined finite volume methods. *Acta Numerica* **2011**, *20*, 211–289.
26. Bonev, B.; Hesthaven, J.S.; Giraldo, F.X.; Kopera, M.A. Discontinuous Galerkin scheme for the spherical shallow water equations with applications to tsunami modeling and prediction. *J. Comput. Phys.* **2018**, *362*, 425–448.
27. Lynett, P.J. Effect of a shallow water obstruction on long wave runup and overland flow velocity. *Journal of Waterway, Port, Coastal, and Ocean Engineering* **2007**, *133*, 455–462.
28. Park, H.; Cox, D.T.; Lynett, P.J.; Wiebe, D.M.; Shin, S. Tsunami inundation modeling in constructed environments: A physical and numerical comparison of free-surface elevation, velocity, and momentum flux. *Coastal Engineering* **2013**, *79*, 9–21.
29. Oishi, Y.; Imamura, F.; Sugawara, D. Near-field tsunami inundation forecast using the parallel TUNAMI-N2 model: Application to the 2011 Tohoku-Oki earthquake combined with source inversions. *Geo. Res. Letters* **2015**, *42*, 1083–1091.
30. Prasetyo, A.; Yasuda, T.; Miyashita, T.; Mori, N. Physical Modeling and Numerical Analysis of Tsunami Inundation in a Coastal City. *Front. Built Environ.* **2019**, *5*, 46–.
31. Kesserwani, G.; Liang, Q. Well-balanced RKDG2 solutions to the shallow water equations over irregular domains with wetting and drying. *Comput. Fluids* **2010**, *39*, 2040 – 2050.
32. Berthon, C.; Marche, F.; Turpault, R. An efficient scheme on wet/dry transitions for shallow water equations with friction. *Comput. Fluids* **2011**, *48*, 192 – 201.
33. Vater, S.; Beisiegel, N.; Behrens, J. A limiter-based well-balanced discontinuous Galerkin method for shallow-water flows with wetting and drying: One-dimensional case. *Advances in Water Resources* **2015**, *85*, 1 – 13.
34. Vater, S.; Beisiegel, N.; Behrens, J. A limiter-based well-balanced discontinuous Galerkin method for shallow-water flows with wetting and drying: Triangular grids. *Int. J. Numer. Methods Fluids* **2019**, *91*, 395–418.
35. Ayog, J.; Kesserwani, G.; Shaw, J.; Sharifian, M.; Bau, D. Second-order discontinuous Galerkin flood model: comparison with industry-standard finite volume models. *Pre-print* **2020**.
36. Lin, P. A numerical study of solitary wave interaction with rectangular obstacles. *Coast. Eng.* **2004**, *51*, 35–51.
37. Apotsos, A.; Jaffe, B.; Gelfenbaum, G. Wave characteristic and morphologic effects on the onshore hydrodynamic response of tsunamis. *Coastal Engineering* **2011**, *58*, 1034–1048.
38. Okal, E.; Synolakis, C. Sequencing of tsunami waves: why the first wave is not always the largest. *Geophys. J. Int.* **2015**, *204*.

39. Lynett, P.; Borrero, J.; Weiss, R.; Greer, D.; Renteria, W. Observations and modeling of tsunami-induced currents in ports and harbors. *Earth Planet. Sci. Lett.* **2012**, *327-328*, 68–74.
40. Borrero, J.; Lynett, P.; Kalligeris, N. Tsunami currents in ports. *Phil. Trans. R. Soc. A* **2015**, *373*, 20140372.
41. Borrero, J.; Synolakis, C.; Fritz, H. Northern Sumatra field survey after the December 2004 Great Sumatra Earthquake and Indian Ocean tsunami. *Earthq. Spectra* **2006**, *22*, S93–S104.
42. Paris, R.; Wassmer, P.; Sartohadi, J.; Lavigne, F., B.B.; Desgages, E.; Grancher, D.; Baumert, P.; Vautier, F.; Brunstein, D.; Gomez, C. Tsunamis as geomorphic crises: lessons from the december 26, 2004 tsunami in Lhok Nga, West Banda Aceh (Sumatra, Indonesia). *Geomorph.* **2009**, *104*, 59–72.
43. Kato, F.; Noguchi, K.; Suwa, Y.; Sakagami, T.; Sato, Y. Field survey on tsunami induced topographical change. *J. Japan Soc. Civil Engrs. Ser. B3* **2012**, *68*, 174–179.
44. Kuriyama, Y.; Takahashi, K.; Yanagishima, S.; Tomita, T. Beach profile change at Hasaki, Japan caused by 5-m-high tsunami due to the 2011 off the Pacific coast of Tohoku earthquake. *Mar. Geol.* **2014**, *355*, 234–243.
45. Yamashita, K.; Sugawara, D.; Takahashi, T.; Imamura, F.; Saito, Y.; Imato, Y.; Kai, T.; Uehara, H.; Kato, T.; Nakata, K.; Saka, R.; Nishikawa, A. Numerical simulations of large-scale sediment transport caused by the 2011 Tohoku earthquake tsunami in Hirota Bay. Southern Sanriku Coast. *Coast. Eng.* **2016**, *58*.
46. Udo, K.; Takeda, Y.; Tanaka, H. Coastal morphology change before and after 2011 off the Pacific coast of Tohoku earthquake tsunami at Rikuzen-Takata coast. *Coast. Eng.* **2016**, *58*, 1640016.
47. Li, L.; Qiu, Q.; Huang, Z. Numerical modeling of the morphological change in Lhok Nga, West Banda Aceh, during the 2004 Indian Ocean tsunami: understanding tsunami deposits using a forward modeling method. *Nat Hazards* **2012**, *64*, 1549–1574.
48. Ontowirjo, B.; Paris, R.; Mano, A. Modeling of coastal erosion and sediment deposition during the 2004 Indian Ocean tsunami in Lhok Nga, Sumatra, Indonesia. *Nat. Hazards* **2013**, *65*, 1967–1979.
49. Sugawara, D.; Takahashi, T.; Imamura, F. Sediment transport due to the 2011 Tohoku-Oki tsunami at Sendai: results from numerical modeling. *Mar. Geol.* **18-37**, *358*, 2014.
50. Qin, X.; Motley, M.; LeVeque, R.; Gonzalez, F.; Mueller, K. A comparison of a two-dimensional depth-averaged flow model and a three-dimensional RANS model for predicting tsunami inundation and fluid forces. *Nat. Hazards Earth Syst. Sci.* **2018**, *18*.
51. OpenFOAM v2.3.1. https://openfoam.org/release/2-3-1/, 2014.
52. Berger, M.; George, D.; LeVeque, R.; Mandli, K. The GeoClaw software for depth-averaged flows with adaptive refinement. *Adv. Water Res.* **2011**, *34*, 1195–1206.
53. Hsiao, S.C.; Lin, T.C. Tsunami-like solitary waves impinging and overtopping an impermeable seawall: Experiment and RANS modeling. *Coastal Engineering* **2010**.
54. Larsen, B.; Fuhrman, D. Full-scale CFD simulation of tsunamis. Part 1: Model validation and run-up. *Coastal Engineering* **2019**, *151*.
55. Larsen, B.; Fuhrman, D. Full-scale CFD simulation of tsunamis. Part 2: Boundary layers and bed shear stresses. *Coastal Engineering* **2019**, *151*.
56. Larsen, B.; Fuhrman, D. On the over-production of turbulence beneath surface waves in Reynold-averaged Navier-Stokes models. *J. Fluid Mech.* **2018**, *853*.
57. Christensen, E. Large eddy simulation of spilling and plunging breakers. *Coastal Eng.* **2006**, *53*, 463–485.
58. Meiburg, E.; Radhakrishnan, S.; Nasr-Azadani, M. Modeling Gravity and Turbidity Currents: Computational Approaches and Challenges. *Appl. Mech. Rev.* **2015**, *67*.
59. Yu, X.; Ozdemir, C.E.; Hsu, T.J.; Balachandar, S. Numerical Investigation of Turbulence Modulation by Sediment-Induced Stratification and Enhanced Viscosity in Oscillatory Flows. *J. Waterway, Port, Coastal, and Ocean Eng.* **2014**, *140*, 160–172.
60. Uhlmann, M. An immersed boundary method with direct forcing for the simulation of particulate flows. *J. Comput. Phys.* **2005**, *209*, 448 – 476.
61. USACE, U.A.C.o.E. Interim Survey Report, Morgan City, Louisiana and Vicinity. Technical Report 63, US Army Engineer District, New Orleans, LA, 1963.
62. Fosberg, F.R.; Chapman, V. Mangroves v. tidal waves. *Biological Conservation* **1971**, *4*, 38–39.
63. Mazda, Y.; Magi, M.; M., K.; Hong, P. Mangroves as a coastal protection from waves in the Tong King Delta, Vietnam. *Mangroves and Salt Marshes* **1997**, *1*.
64. Möller, I.; T., S.; J.R., F.; Leggett, D.; Dixon, M. Wave transformation over salt marshes: A field and numerical modeling study from North Norfolk, England. *Estuar Coast Shelf Sci.* **1999**, *49*.

65. Harada, K.; Imamura, F. Effects of coastal forest on tsunami hazard mitigation - a preliminary investigation. In *Tsunamis*; Springer, 2005; pp. 279–292.
66. Tanaka, N.; Sasaki, Y.; Mowjood, M.; Jinadasa, K.; Homchuen, S. Coastal vegetation structures and their functions in tsunami protection: experience of the recent Indian Ocean tsunami. *Landscape and Ecological Engineering* **2007**, *3*, 33–45.
67. Tanaka, N.; Nandasena, N.; Jinadasa, K.; Sasaki, Y.; Tanimoto, K.; Mowjood, M. Developing effective vegetation bioshield for tsunami protection. *Civil Engineering and Environmental Systems* **2009**, *26*, 163–180.
68. Stoesser, T.; Palau Salavador, G.; Rodi, W.; Diplas, P. Large eddy simulation of flow through submerged vegetation. *Transp. Porous. Med.* **2009**, *78*, 347–365.
69. Iimura, K.; Tanaka, N. Numerical simulation estimating effects of tree density distribution in coastal forest on tsunami mitigation. *Ocean Engineering* **2012**, *54*, 223–232.
70. Tanaka, N.; Jinadasa, K.; Mowjood, M.; Fasly, M. Coastal vegetation planting projects for tsunami disaster mitigation: effectiveness evaluation of new establishments. *Landscape and ecological engineering* **2011**, *7*, 127–135.
71. Tanaka, N. Effectiveness and limitations of vegetation bioshield in coast for tsunami disaster mitigagation. In *The tsunami threat-research and technology*; InTech, 2011.
72. Thuy, N.B.; Tanaka, N.; Tanimoto, K. Tsunami mitigation by coastal vegetation considering the effect of tree breaking. *Journal of coastal conservation* **2012**, *16*, 111–121.
73. Nepf, H. Drag, turbulence, and diffusion in flow through emergent vegetation. *Water Resources Res.* **1999**, *35*, 479–489.
74. Bayas, J.; Marohn, C.; Dercon, G.; Dewi, S.; Piepho, H.; Joshi, L.; van Noordwijk, M.; Cadisch, g. Influence of coastal vegetation on the 2004 tsunami wave impact in West Aceh. *Proceedings of the National Academy of Sciences - PNAS* **2011**, *108*, 18612–18617.
75. Westerink, J.; Luettich, R.; Baptista, A.; Scheffner, N.; Farrar, P. Tide and storm surge predictions using finite element model. *ASCE J. Hydraul. Eng* **1992**, *118*.
76. Kanoglu, U.and Synolakis, C. Long wave runup on piecewise linear topographies. *J. Fluid Mech.* **1998**, *374*.
77. Westerink, J.; Luettich, R.; Feyen, J.; Atkinson, J.; Dawson, C.; Roberts, H.; Powell, M.; Dunion, J.; Kubatko, E.; Pourtaheri, H. A basin-to-channel-scale unstructured grid hurricane storm surge model applied to southern Louisiana. *Mon. Wea. Rev.* **2008**, *136*.
78. Sun, F.; Carson, R. Coastal wetlands reduce property damage during tropical cyclones. *Proceedings of the National Academy of Sciences - PNAS* **2020**, *117*, 5719–5725.
79. Jackson, N.; Nordstrom, K.; Feagin, R.; Smith, W. Coastal geomorphology and restoration. *Geomorph.* **2013**, *199*.
80. Day, J.; Boesch, D.; Clairain, E.e.a. Restoration of the Mississippi Delta: Lessons from Hurricanes Katrina and Rita. *Science* **2007**, *315*.
81. Gedan, K.; Kirwan, M.; Wolanski, E.; Barbier, E.; Silliman, B. The present and future role of coastal wetland vegetation in protecting shorelines: Answering recent challenges to the paradigm. *Clim. Change* **2011**, *106*.
82. Shephard, C.; Crain, C.; Beck, M. The protective role of coastal marshes: A systematic review and meta-analysis. *PLoS ONE* **2012**, *6-e27374*.
83. Horstman, E.; Dohmen-Janssen, C.; Narra, P.; van den Berg, N.; Siemerink, M.; Hulscher, S. Wave attenuation in mangroves: A quantitative approach to field observations. *Coast. Eng.* **2014**, *94*.
84. Mattis, S.; Dawson, C.; Kees, C.; Farthing, M. An immersed structure approach for fluid-vegetation interaction. *Adv. Water Res.* **2015**, *80*.
85. Mattis, S.; Kees, C.; Wei, M.; Dimakopoulos, A.; Dawson, C.N. Computational Model for Wave Attenuation by Flexible Vegetation. *Journal of Waterway, Port, Coastal, and Ocean Engineering* **2019**, *145*, 04018033.
86. Mukherjee, A.; Cajas, J.; Houzeaux, G.; Lehmkuhl, O.; Vázquez, M.; Suckale, J.; Marras, S. Using fluid-structure interaction to evaluate the energy dissipation of a tsunami run-up through idealized flexible trees. *sciencesconf.org:parcfd2020:320200* **2020**.
87. Lin, P.; Liu, P. A numerical study of breaking waves in the surf zone. *J. Fluid Mech.* **1998**, *358*, 239–264.
88. Lin, P.; Liu, P. Turbulence transport, vorticity dynamics, and solute mixing under plunging breaking waves in surf zone. *J. Geophys. Res.* **1998**, *103 C8*.
89. Horrillo, J.; Wood, A.; Kim, G.; Parambath, A. A simplified 3-D /Navier–Stokes numerical model for landslide tsunami: Application to the Gulf of Mexico. *J. Geophys. Res./Oceans* **2013**, *118*, 6934–6950.

90. Zhang, Y.; Ye, F.; Stanev, E.; Grashorn, S. Seamless cross-scale modeling with SCHISM, Ocean Modelling. *Ocean Model.* **2016**, *102*, 64–81.
91. Jacobsen, N.; Fuhrman, D.; Fredsoe, J. A wave generation toolbox for the open-source CFD library: OpenFOAM (R). *Int. J. Numer. Methods Fluids* **2012**, *70*, 1073–1088.
92. Ghosh, D.; Mittal, A.; Bhattacharyya, S. Multiphase modeling of tsunami impact on building with openings. *J. Comput. Multiph. Flows* **2016**, *8*, 85–94.
93. Owen, H.; Houzeaux, G.; Samaniego, C.; Cucchietti, F.; Marin, G.; Tripiana, C.; H., C.; Vázquez, M. Two Fluids Level Set: High Performance Simulation and Post Processing. *IHigh Performance Computing, Networking, Storage and Analysis (SCC) IEEE Conference* **2012**.
94. Marras, S.; Suckale, J.; Lunghino, B.; Giraldo, F.; Hood, K.M. Quantifying the role of mitigation hills in reducing tsunami runup. AGU Fall Meeting Abstracts, 2015, Vol. 2015, pp. NH23C–1904.
95. Mandli, K. A numerical method for the two layer shallow water equations with dry states. *Ocean Model.* **2013**, *72*, 80–91.
96. Giraldo, F.X.; Restelli, M. A Conservative Discontinuous Galerkin Semi-Implicit Formulation for the Navier-Stokes Equations in Nonhydrostatic Mesoscale Modeling. *SIAM J. Sci. Comp.* **2009**, *31*, 2231–2257.
97. Marras, S.; Kopera, M.; Giraldo, F.X. Simulation of Shallow Water Jets with a Unified Element-based Continuous/Discontinuous Galerkin Model with Grid Flexibility on the Sphere. *Q. J. Roy. Meteor. Soc.* **2015**, *141*, 1727–1739.
98. Marras, S.; Kopera, M.; Constantinescu, E.; Suckale, J.; Giraldo, F. A Residual-based Shock Capturing Scheme for the Continuous/Discontinuous Spectral Element Solution of the 2D Shallow Water Equations. *Adv. Water Res.* **2018**, *114*, 45–63.
99. Titov, V.V.; Gonzalez, F. Implementation and testing of the Method Of Splitting Tsunami(MOST) model. NOAA Technical Memorandum ERL PMEL-112 1927, NOAA, Seattle, WA,USA. Technical report, 1997.
100. Imamura, F.; Yalciner, A.; Ozyurt, G. Tsunami Modelling Manual. Technical report, 2006.
101. Yalciner, A.; Pelinovsky, E.; Zaytsev, A.; Kurkin, A.; Ozer, C.; Karakus, H. NAMI DANCE Manual. Technical report, METU, Civil Engineering Department, Ocean Engineering Research Center, Ankara, Turkey, 2006.
102. Wang, X. User manual for COMCOT version 1.7. Technical report, 2009.
103. Gailler, A.; Hbert, H.; Loevenbruck, A.; Hernandez, B. Simulation systems for tsunami wave propagation forecasting within the French tsunami warning system. *Nat. Hazards Earth Sys. Sci.* **2013**, *13*, 2465–2482.
104. Reymond, D.; Okal, E.A. Hébert, H.; Bourdet, M. Rapid forecast of tsunami wave heights from a database of pre-computed simulations, and application during the 2011 Tohoku tsunami in French Polynesia. *Geophys. Res. Lett.* **2012**, *39*, 39.
105. Zhang, Y.; A.M., B. An efficient and robust tsunami model on unstructured grids. Part I: inundation benchmarks. *Pure Appl. Geophys.* **2008**, *165*, 2229–2248.
106. Harig, S.; Chaeroni, X.; Pranowo, W.; Behrens, J. Tsunami simulations on several scales: comparison of approaches with unstructured meshes and nested grids. *Ocean Dyn.* **2008**, *58*, 429–440.
107. Dutykh, D.; Poncet, R.; Dias, F. The VOLNA code for the numerical modeling oftsunami waves: generation, propagation and inundation. *Eur. J. Mech. B/Fluids* **2011**, *30*, 598–615.
108. Pranowo, W.; Behrens, J.; Schlicht, J.; Ziemer, C. Adaptive mesh refinement applied to tsunami modeling: TsunaFLASH. 2008.
109. Roelvink, J.; Van Banning, G. Design and development of DELFT3D and application to coastal morphodynamics. *Oceanographic Lit. Review* **1995**, *42*, 925–.
110. Popinet, S. Basilisk: simple abstractions for octree-adaptive scheme. SIAM conference on Parallel Processing for Scientific Computing. April 12-15; , 2016.
111. Kennedy, A.; Chen, Q.; Kirby, J.; Dalrymple, R. Boussinesq modeling of wave transformation, breaking and runup, part I: 1D. *J. Waterw. Port Coast. Ocean Eng.* **2000**, *126*, 39–47.
112. Shi, F.; Kirby, J.; Harris, J.; Geiman, J.; Grilli, S. A high-order adaptive time-stepping TVD solver for Boussinesq modeling of breaking waves and coastal inundation. *Ocean Model.* **2012**, *43-44*, 36–51.
113. Lynett, P.; Wu, T.; P.L.F., L. Modeling wave runup with depth-integrated equations. *Coast. Eng.* **2002**, *46*, 89–107.
114. Kim, D.; Lynett, P. Turbulent mixing and passive scalar transport in shallow flows. *Phys. Fluids* **2011**, *23*, 016603.

115. Yamazaki, Y.; Kowalik, Z.; Cheung, K. Depth-integrated, non-hydrostatic model for wave breaking and run-up. *Int. J. Numer. Meth. Fluids* **2009**, *61*, 473–497.
116. Wei, Z.; Dalrympl, R.; Hérault, A.; Bilotta, G.; Rustico, E.; Yeh, H. SPH modeling of dynamic impact of tsunami bore on bridge pier. *Coast. Eng.* **2015**, *104*, 26–42.
117. Vázquez, M.; Houzeaux, G. Alya: Multiphysics Engineering Simulation Towards Exascale. *J. Comput. Sci* **2016**.
118. George, D.L.; LeVeque, R.L. Finite volume methods and adaptive refinement for global tsunami propagation and local inundation. *Sci. Tsunami Hazards* **2006**, *24*, 319–328.
119. Marras, S.; Suckale, J.; Eguzkitza, B.; Houzeaux, G.; Vázquez, M.; Owen, H. Large Eddy Simulation of Tsunami Triggered Coastal Inundation in the Presence of Mitigation Parks. *PASC2018: The Platform for Advanced Scientific Computing (PASC) Conference* **2018**.
120. Behrens, J. *Adaptive atmospheric modeling. Key techniques in grid generation, data structures, and numerical operations with applications*; Springer, 2006; p. 207.
121. Müller, A.; Kopera, M.; Marras, S.; Wilcox, L.; Isaac, T.; Giraldo, F. Strong scaling for numerical weather prediction at petascale with the atmospheric model NUMA. *Int. J. High Perform. Comput.* **2018**. doi:10.1177/1094342018763966.
122. Abdi, D.; Giraldo, F.; E. Constantinescu, C.L.I.; Wilcox, L.; Warburton, T. Acceleration of the Implicit-Explicit Non-Hydrostatic Unified Model of the Atmosphere (NUMA) on Manycore Processors. *Int. J. High Perform. Comput.* **2017**. doi:10.1177/1094342017732395.
123. Bunya, S.; Kubatko, E.J.; Westerink, J.J.; Dawson, C. A wetting and drying treatment for the Runge–Kutta discontinuous Galerkin solution to the shallow water equations. *Computer Methods in Applied Mechanics and Engineering* **2009**, *198*, 1548 – 1562.
124. Madden, E.; Bader, M.; Behrens, J.; van Dinther, Y.; Gabriel, A.A.; Rannabauer, L.; Ulrich, T.; Uphoff, C.; Vater, S.; Wollherr, S.; van Zelst, I. Linked 3D modeling of megathrust earthquake-tsunami events: from subduction to tsunami run up. *Geophysical Journal International* **2020**. preprint, in press, doi:10.31223/osf.io/rzvn2.
125. Bungartz, H.; Lindner, F.; Gatzhammer, B.; Mehl, M.; Scheufele, K.; Shukaev, A.; Uekermann, B. preCICE–a fully parallel library for multi-physics surface coupling. *Computers & Fluids* **2016**, *141*, 250–258.
126. Mehl, M.; Uekermann, B.; Bijl, H.; Blom, D.; Gatzhammer, B.; Van Zuijlen, A. Parallel coupling numerics for partitioned fluid–structure interaction simulations. *Comput. & Math. Appl.* **2016**, *71*, 869–891.
127. Lotto, G.; Jeppson, T.; Dunham, E. Fully Coupled Simulations of Megathrust Earthquakes and Tsunamis in the Japan Trench, Nankai Trough, and Cascadia Subduction Zone. *Pure Appl. Geophys.* **2019**, *176*, 4009–4041.
128. ASCETE. Advanced Simulation of Coupled Earthquake and Tsunami Events. https://t3projects.cen.uni-hamburg.de/index.php?id=2099.